03 Sep 2020

Peritectic Behavior Detection in the Fe-C-Mn-Al-Si Steel System using Fiber Optic Temperature Mapping

Muhammad Roman

Damilola Balogun

Rex E. Gerald II

Laura Bartlett
Missouri University of Science and Technology, lnmkvf@mst.edu

et. al. For a complete list of authors, see https://scholarsmine.mst.edu/matsci_eng_facwork/2700

Recommended Citation

M. Roman et al., "Peritectic Behavior Detection in the Fe-C-Mn-Al-Si Steel System using Fiber Optic Temperature Mapping," *Proceedings of the AISTech 2020 (2020, Cleveland, OH)*, pp. 822-833, Association for Iron & Steel Technology (AIST), Sep 2020.
The definitive version is available at https://doi.org/10.33313/380/087

DOI 10.33313/380/087

Peritectic Behavior Detection in the Fe-C-Mn-Al-Si Steel System Using Fiber Optic Temperature Mapping

Muhammad Roman [1], Damilola Balogun [2], Rex E. Gerald II [1], Laura Bartlett [2], Jie Huang [1] and Ronald J. O'Malley [2]

[1]Department of Electrical and Computer Engineering, Missouri University of Science and Technology, Rolla, MO 65409, USA
mrhmc@mst.edu ; geraldr@mst.edu; jieh@mst.edu

[2]Department of Material Science and Engineering, Missouri University of Science and Technology, Rolla, MO 65409, USA
dsbcrh@mst.edu ; lnmkvf@mst.edu; omalleyr@mst.edu

ABSTRACT

Peritectic reactions can cause surface defects and breakouts in continuous casting and the peritectic region is often avoided by adjusting the chemical composition of the steel to cast outside of the peritectic sensitivity range. However, the combined effects of C, Mn, Al, and Si on the boundaries that map peritectic region are still disputed for many advanced high strength steel grades. An apparatus for performing controlled solidification experiments is being developed to characterize the effects of chemical composition on the uniformity of shell growth during solidification using a copper chill mold with an embedded fiber-optic temperature sensor that enables high spatial resolution temperature mapping. The spatially distributed fiber-optic sensor employs optical frequency domain reflectometry to measure temperatures with a 0.6mm spatial resolution along the length of the fiber at a 20ms sampling rate to map closely spaced temperature features caused by the peritectic reaction. This paper reports progress on the ongoing efforts to develop a peritectic sensing system using optical fiber temperature sensing technology.

Keywords: Peritectic Reaction, Temperature Sensor, Optical Fiber, Optical Frequency Domain Reflectometry, Distributed Sensing

INTRODUCTION

The continuous casting of peritectic medium carbon steel has always been very challenging given the fact that such steel grades are more prone to surface cracks. The shrinkage caused by the δ/γ phase transformation during the initial solidification of peritectic steel grades can induce shell buckling which in turn causes uneven shell formation, non-uniform shell and mold temperatures, and an average decrease in heat flux from shell to the mold [1]. Various attempts have been made to investigate peritectic behavior using thermodynamic modeling software to predict the shift in the peritectic sensitivity range as a function of steel composition [2]. It has been demonstrated that the peritectic sensitivity range in Fe-C alloys is strongly affected by the addition of alloying elements such as silicon, manganese and aluminum [3]. The combined effects of these elements on the compositions that exhibit peritectic behavior are not well predicted by these models and little experimental work has been done to document the peritectic sensitivity ranges in AHS steels containing higher levels of Mn, Si, and Al.

The application of fiber optics for the characterization of peritectic behavior is promising because fiber optic based temperature sensing can provide an accurate, high spatial resolution, distributed, fast, and minimally invasive temperature measurement system that is highly desirable for this application. Temperature measurements in steel industry applications are commonly performed with thermocouples [4][5][6][7]. Thermocouples provide reliable and fast temperature measurements with good accuracy and high-temperature resolution. However, they have several limitations because they only provide single point measurements, which makes them less suited for applications that exhibit closely spaced fluctuating temperature features.

Temperature mapping using multiple thermocouples makes the system cumbersome due to the large number of lead wires needed to interrogate them. Moreover, the size of the thermocouple probe often requires a significant modification to the device under measurement, possibly interfering with the desired measurement or compromising the structural integrity of the mold. These thermocouples are also susceptible to electromagnetic interference.

The aforementioned limitations of thermocouples has motivated researchers to look for alternative sensing technologies. Optical fiber technologies have emerged as promising sensing solutions due to the miniaturized size of the optical waveguide, immunity to electromagnetic interference, the ability to withstand harsh environments, and the capability for high resolution distributed sensing along the length of the fiber [8][9]. Several optical fiber-based sensors for temperature measurement have been reported. Fiber-optic interferometers are commonly exploited for temperature measurement [10]. Interferometers offer high sensitivity and good temperature resolution but they can only provide point measurements like thermocouples. Fiber-optic distributed temperature sensors based on optical time domain reflectometry (OTDR) have been widely studied [11]–[14]. These OTDR based sensors offer a spatial resolution of the order of a few meters along the length of the fiber, which is not suitable for measuring closely spaced temperature features in a caster mold, such as those observed in peritectic behavior. Fiber Bragg gratings (FBGs) are also used for distributed temperature sensing [15]–[18]. FBGs have attracted considerable interest in the steelmaking industry due to a quasi-distributed sensing capability with reasonable spatial resolution (~1 cm), high-temperature sensitivity (~10 pm/°C) and fast measurement rates (~5kHz). B.G. Thomas and M.K. Okelman reported results using a casting mold with embedded FBG sensors for temperature and strain measurements [19]. The FBG sensors were embedded in a copper mold using a nickel electroplating process. Temperature variations were recorded 1 mm away from the hotface in a laboratory simulations of the continuous casting process. Lieftucht et al. developed a mold embedded with FBGs for temperature measurements in the continuous casting process of steel [20]. Temperature profiles were used to calculate mold levels and local heat flux readings. Spierings et al. designed a mold by embedding FBGs in the upper half of a copper mold plate with 2,660 temperature measurement points [21]. The instrumented mold was tested on different steel grades. Temperature measurements were used to observe fluid flow and mold thermal behavior. Currently, there are several companies offering commercial systems for mold thermal monitoring based on FBG optical fiber technology.

Although FBGs offer better spatial resolution than OTDR, they have other limitations. For example, FBGs are not truly distributed and they only afford quasi-distributed sensing. Moreover, FBGs require modifications to single mode fibers to create the gratings, which adds to the cost of the fiber. Another known disadvantage of FBGs is their inability to withstand temperatures exceeding 700 °C, as the grating features can become diffuse at elevated temperatures. Optical frequency domain reflectometry (OFDR) based on Rayleigh scattering is another fiber-optic distributed temperature sensing solution [22][23]. OFDR systems employ un-modified single mode optical fibers as sensor devices. Moreover, OFDR systems offer spatial resolution in the range of submillimeter to few millimeters with fast measurement rates. The distributed sensing capability with high spatial resolution and fast update rates make OFDR an exciting prospect for the characterization of peritectic phenomena that involve closely spaced temperature features.

In this work, OFDR systems are employed to perform fiber-optic distributed temperature measurements. Moreover, experiments were designed and conducted to provide evidence that Rayleigh scattering based fiber-optic temperature sensors, due to high spatial resolution and fast measurement rates of OFDR systems, are a suitable candidates for thermal mapping of the phenomena that involve closely spaced temperature features, such as peritectic behavior. The measurement capability and survivability of fiber-optic temperature sensors in a mold subjected to immersion in molten steel was also tested. A dip test was performed using a copper chill block with embedded optical fibers. Temperature distributions along the length of the mold surface were measured during shell formation. The experimental results showed that the distributed fiber-optic temperature measurement is a viable candidate for thermal mapping of the mold during the solidification process, and efforts to apply the technology for mapping peritectic sensitivity ranges for steels containing varying levels of C, Mn, Si, and Al are ongoing.

FIBER-OPTIC TEMPERATURE SENSING PRINCIPLE AND INTERROGATION SYSTEM

Optical Fiber

The sensor head for temperature measurements consists of a single mode optical fiber (SMF) . The optical fiber is a dielectric waveguide made of a germanium-doped silica core, surrounded by a silica cladding as shown in Figure 1. The typical core diameter in SMF is 8-10 μm, while that of cladding is 125 μm. The fiber is coated with a polymer material (typically acrylate or polyimide) to provide mechanical strength. The core of the fiber has a slightly higher refractive index than the refractive index of cladding due to germanium doping in the core. The refractive index contrast between core and cladding ensures total internal reflection which is the basis of light confinement and guidance in the core of the fiber.

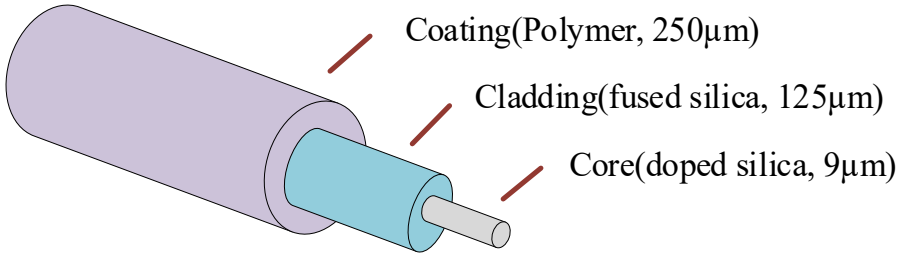

Figure 1. Structure of the standard single mode optical fiber.

Rayleigh Scattering Based Temperature Measurements

The proposed system of distributed temperature measurements is based on Rayleigh scattering in a single-mode optical fiber. Rayleigh scattering originates when light strikes an inhomogeneity in a continuum of matter with dimensions smaller than the wavelength of light. In an optical fiber, random fluctuations in the refractive index of the optical fiber material (glass) cause Rayleigh scattering. Temperature variations cause changes in the refractive index and the length of the optical fiber, which in turn results in shifts in the locally reflected Rayleigh backscattering (RBS) spectra. The RBS shift Δλ caused by a temperature change ΔT can be expressed as

$$\frac{\Delta\lambda}{\lambda} = (\alpha + \xi)\Delta T \quad (1)$$

where α is the thermal expansion coefficient and ξ is the thermo-optic coefficient of the optical fiber material. The value of the thermal expansion coefficient is 0.55×10^{-6} /°C, while that of the thermo-optic coefficient is 8.5×10^{-6} /°C. As the value of the thermal expansion coefficient is approximately an order of magnitude smaller than the thermo-optic coefficient, the spectrum shift due to temperature variations is usually attributed to the change in refractive index.

Optical Frequency Domain Reflectometry (OFDR)

OFDR is the interrogator system used to acquire, process, and analyze backscattered light. In an OFDR system, light from a tunable laser source is launched into an optical fiber network containing an interferometer. The interference signal from the interferometer is detected and analyzed. As shown in the schematic of the OFDR system we developed in our laboratory (Figure 2), light from a tunable laser source (LUNA PHOENIX™ 1200) with a 50 nm tuning range (1515 nm–1565 nm) and a 1000 nm/s tuning speed is launched into an optical fiber network. The first 3 dB coupler splits the incident light between the two arms—one beam going into an auxiliary interferometer and the other beam going into the main interferometer. The auxiliary interferometer is used as a clock generator for the data acquisition card in order to compensate for the nonlinear sweep of the laser. The main interferometer is a Mach-Zehnder interferometer with two arms, one used as a reference arm and the other as a sensing arm. Backscattered light from the sensing arm combines with the reference signal in a 50-50 coupler and generates an interference signal, which is collected by a data acquisition card and then transmitted to a computer. Temperatures metered along the longitudinal spatial dimension of the optical fiber are retrieved through a series of signal processing steps.

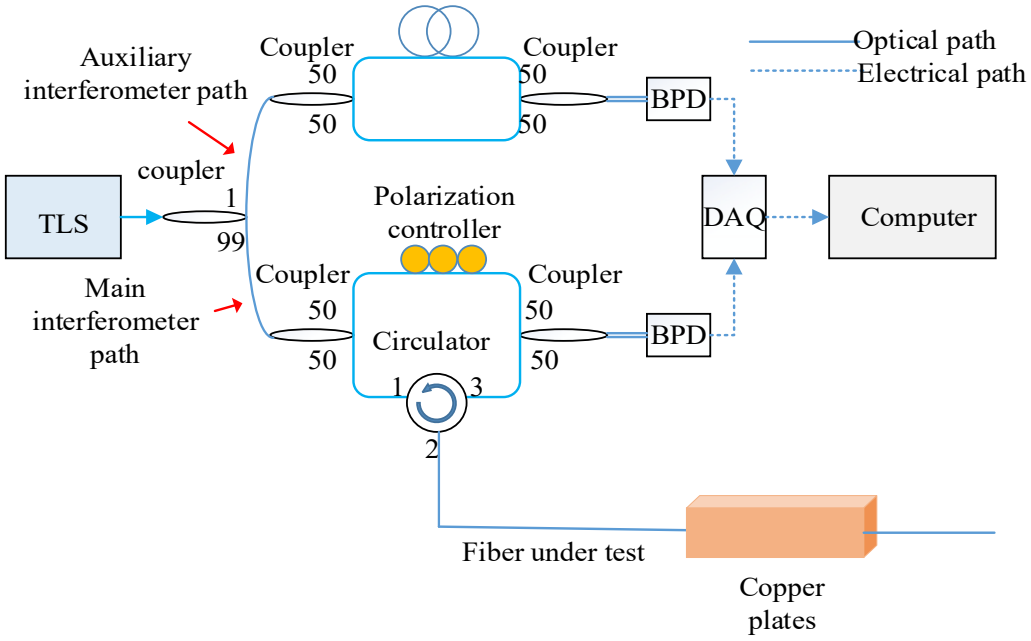

Figure 2. A schematic diagram of the optical frequency domain reflectometry system. TLS: tunable laser source, BPD: balanced photodetector, DAQ: data acquisition card.

EVALUATION OF OPTICAL FIBERS FOR MOLD TEMPERATURE MEASUREMENT

A 2D thermal mapping experiment was performed using the copper plate into which a cavity was machined as shown in Figure 3. A single strand of continuous optical fiber was placed in direct contact with the mold in eight parallel paths, each separated by 2 mm, on the copper plate as shown in Figure 3(a). The copper plate was then heated on a hot plate. Temperature measurements were conducted with 0.65 mm spatial resolution and a fiber interrogation rate of 40Hz. The temperature distribution along fiber sections passing through flat surface exhibited a uniform temperature, while the fiber sections bridging the air bubble exhibited dips in temperature profiles as depicted in Figure 3(b). This experiment demonstrated that the optical fiber was able to distinguish closely spaced temperature gradients. However, other experiments were also conducted with fibers placed loosely into machined grooves and embedded tubes. These tests confirmed the importance of maintaining good thermal contact between the fiber and the mold without binding the fiber or imparting strain to it.

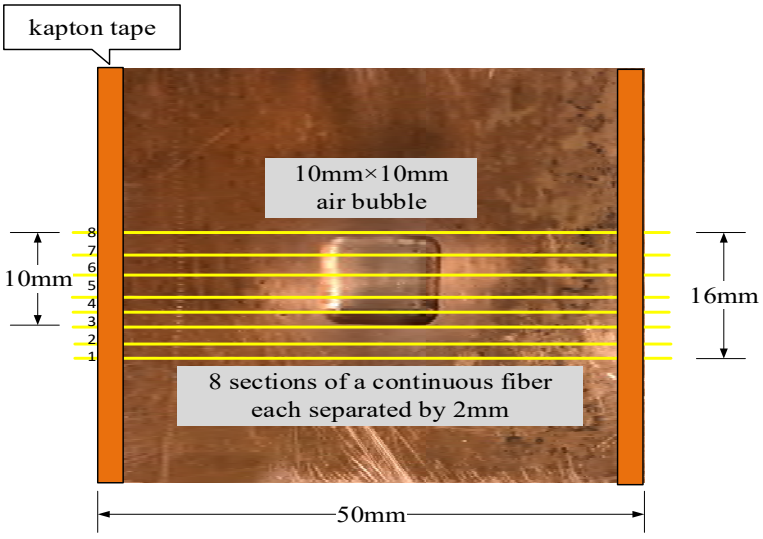

(a)

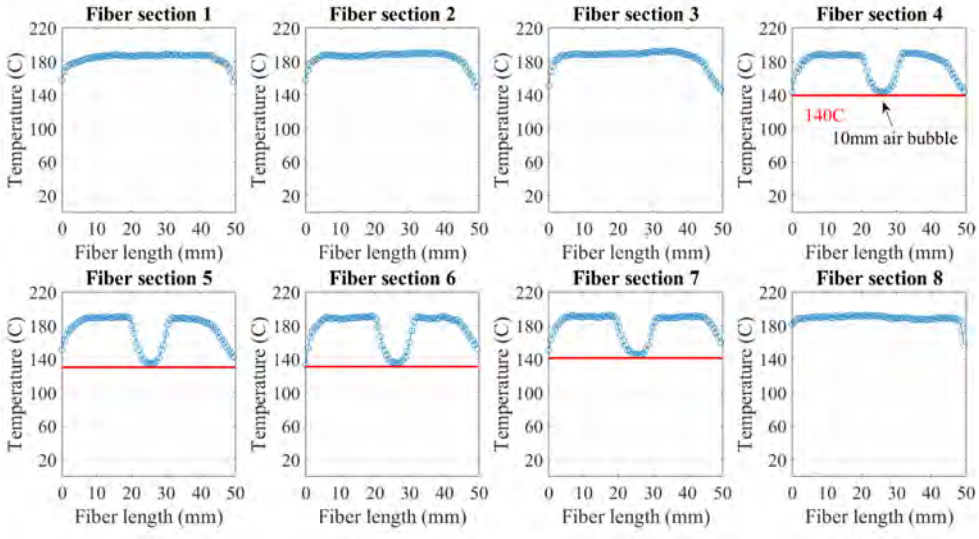

(b)

Figure 3. 2D thermal mapping on the test plate. (a) Arrangement of eight sections of a looped continuous fiber on the model copper plate. Four of the fiber sections are in contact with the flat surface of the plate, while the other four fiber sections pass through the machined cavity. (b) Temperature distribution along eight sections of the optical fiber. The fiber sections passing through the cavity exhibited a dip in the spatial temperature profile.

The thermal map of the plate matched well with the dimensions of the machined cavity in the copper plate as shown in Figure 4. The dimensions of the low temperature region shown in Figure 4(b) corresponds to the physical dimensions of the air bubble on the plate shown in Figure 4(a).

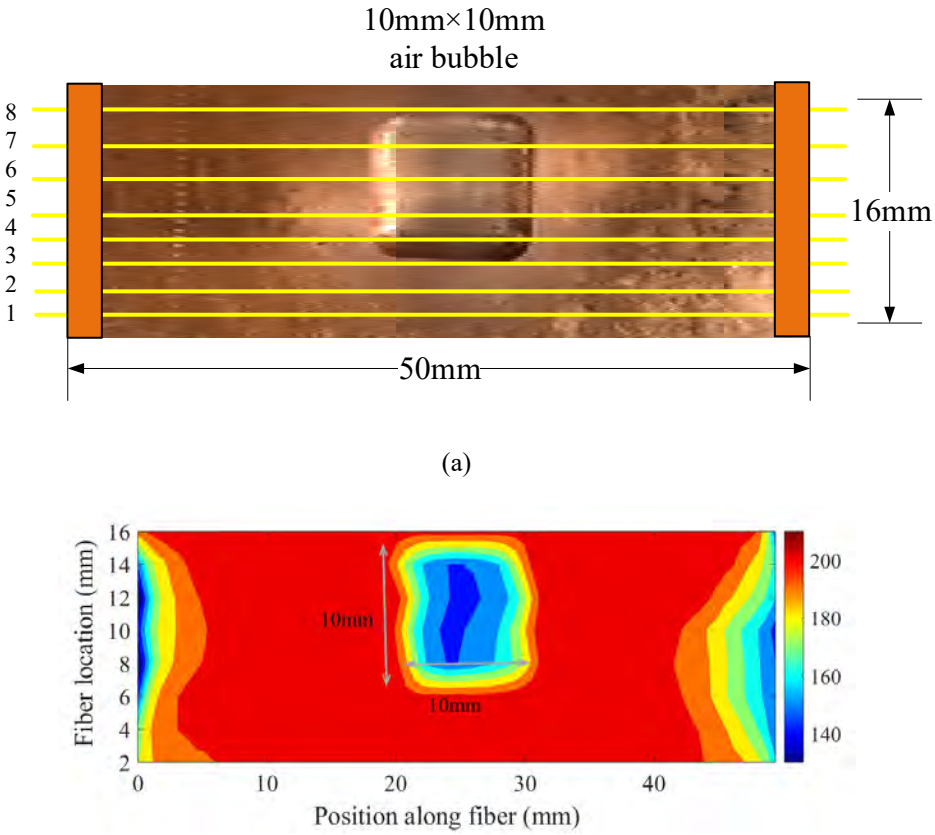

Figure 4. Thermal mapping of the sheet model. (a) Arrangement of optical fibers on a copper sheet with an air bubble in the middle. (b) Thermal map of the sheet model. The low temperature feature is due to air bubble.

The experimental simulation of the peritectic-like phenomenon provided strong evidence that the Rayleigh scattering based fiber-optic temperature sensors can measure temperature features in a mold associated with peritectic behavior. The spatially continuous thermal maps of the mold during solidification can help to monitor rapid and closely spaced thermal events at the meniscus that are attributed to the peritectic reaction. To demonstrate the spatially continuous temperature measurement capability of the system during solidification, a dip test was also performed on a low carbon steel grade with chemistry shown in Table 1 that will be part of a future study with varying levels of C, Mn, Si, and Al.

Table 1. Composition of Steel Used to Demonstrate Optical Fiber Temperature Sensing Capabilities

Alloy (wt. %)	Fe	C	Mn	Al	Si
	Bal.	0.05	0.05	0.05	0.05

PRELIMINARY DIP TEST EVALUATIONS

The apparatus used for the dip testing evaluations is shown in Figure 5. The apparatus consists of a frame that can be moved into position over a 200 lb. induction furnace and perform a controlled immersion of a chill mold into a molten steel bath. The chill mold is housed within a paddle which serves to protect the embedded optical fiber during immersion into the steel bath. The paddle is connected to a stepper motor that controls the immersion timing cycle for the mold using a programmable stepper motor. The programmable stepper is based on a servo mechanism in which a drive connected to a computer via Ethernet cable controls all the motion parameters including speed of immersion, dwell time of paddle in molten bath and speed

of withdrawal from the molten bath. The parameters are summarized in table 2. The paddle was withdrawn from the melt at the same rate it was immersed and the solidified shell was recovered after the test.

Table 2. Dip test motion parameters.

Rate of immersion	Dwell time in `bath	Rate of withdrawal from bath
40 mm/s	4 sec	40 mm/s

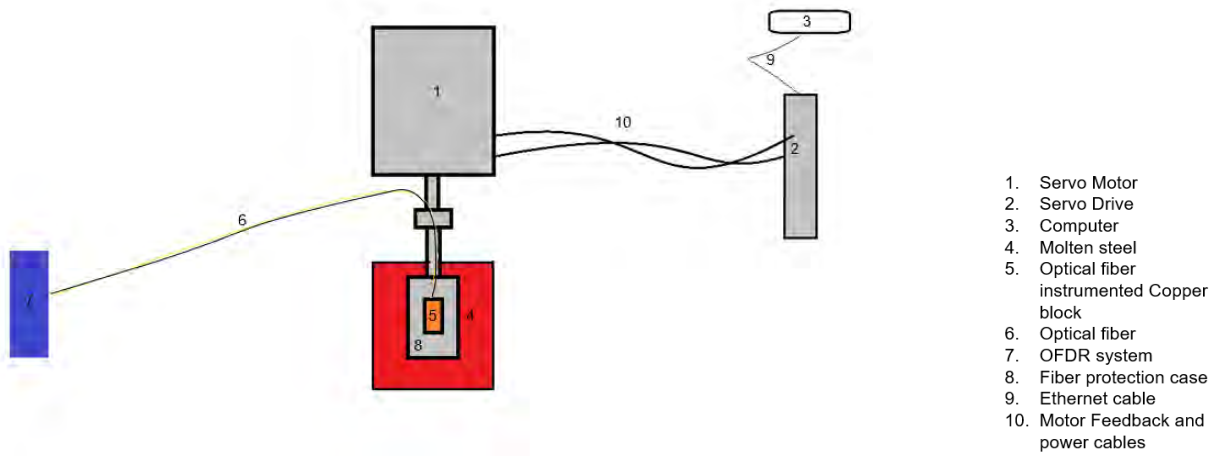

Figure 5. Schematic of dip test apparatus with programmable devices to control motion of paddle and OFDR system for acquiring measurement signal

In this preliminary test, the copper chill block used for the dip test was instrumented with two optical fibers for temperature measurements to evaluate a potential fiber embedding method. To embed optical fibers into the block, two deep 350µm wide slots were machined longitudinally from the back face of a copper block (100 mm x 50 mm x 12 mm thick) to within 1 mm of the hot face using wire EDM. The optical fibers were loosely placed at the base of the slot, which was then back filled with copper powder (325 mesh). The schematic of the copper block with embedded optical fibers is shown in Figure 6.

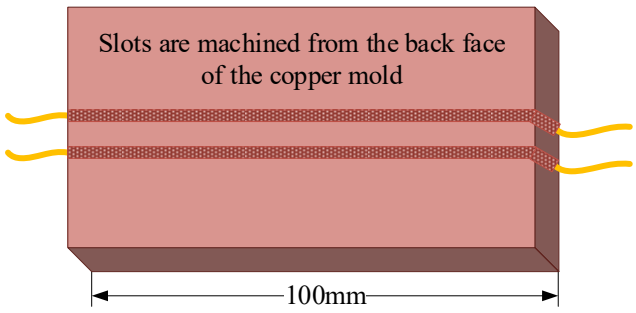

Figure 6. A schematic of the copper chill block with embedded optical fibers. Two slots, each 350µm wide, were machined from the back face of the copper block. Fibers were placed at the root of the slots. The slots were then filled with the copper powder to promote good thermal contact with the plate without binding the fiber.

This embedding technique helped to achieve three objectives. The use of thin machined slots from the back face of the block minimized interference with the hot face heat flow in the mold, thus providing a more uniform surface to be exposed to the molten steel. The deep slots ensured that optical fibers close to the hot face to allow them to capture rapid thermal events. The loose fiber surrounded by copper powder provided improved heat flow uniformity while ensuring that no thermally induced strain was transferred to the optical fiber from the copper block as it heated.

The measured distributed temperature profile along the copper mold during immersion and solidification is shown in Figure 7. A temperature rise is observed during immersion and a gradient in temperature is also observed along the length of the mold. The middle part of the mold registered a higher temperature than the region near the upper and lower edges of the block. It is possible that this behavior results from lifting of the shell from the mold at its edges during shell growth. The length of the copper mold assembly is 100mm, while the length exposed to the molten steel is 70mm. The part of the block which is not exposed to the molten metal (15mm length at the top and 15mm at the bottom) can also experience thermal gradients by extracting heat from the exposed portion of the block. Temperature gradients started to dissipate shortly after the block was removed from the molten steel.

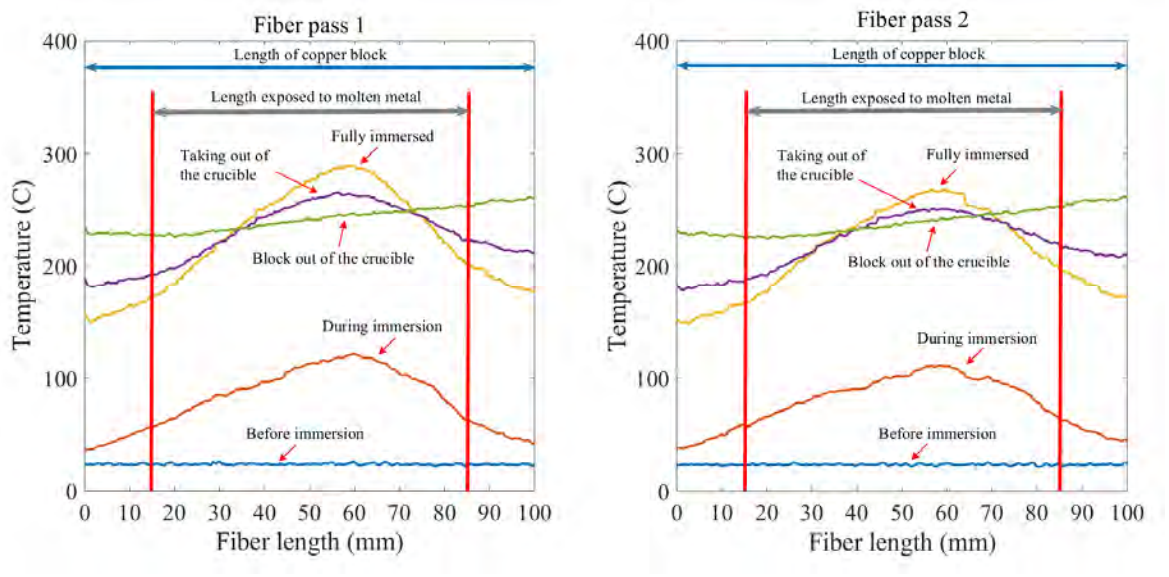

Figure 7. Temperature distribution along the copper mold during dip test. Two fiber sections are at 1mm away from the hot face.

Temperature variations at three different locations on the fiber along the mold are shown in Figure 8. It is evident from the temperature profile that middle part of the mold exhibited a higher heating rate than the regions near the edge of the chill plate.

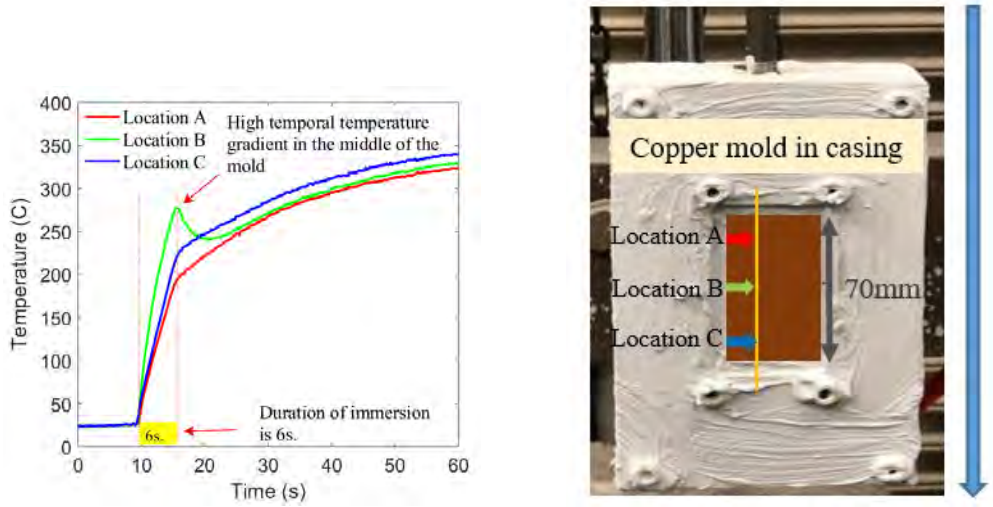

(a) (b)

Figure 8. Temperature measurements at three locations of the mold. (a) A copper chill block fixed in a metal casing for dip test. (b) Temperature profiles over time at three different locations of the mold. The locations are marked in part (a).

Concurrently, a method for characterizing the thickness variation in the shell sample was employed in order to compare the shell thickness profiles to the mold thermal mapping results. This method, which is still being developed and verified, has provided some interesting information about the shell thickness non-uniformity which makes it a potential technique for observing the peritectic behavior independently from the thermal mapping method. To test these ideas, the steel shell produced from the dip test was cleaned and scanned using an OptimScan-5M metrology grade 3D scanner with 0.04 mm resolution. Scanning was done by mounting the shell on a rotating turntable with the orientation shown in Figure 9.

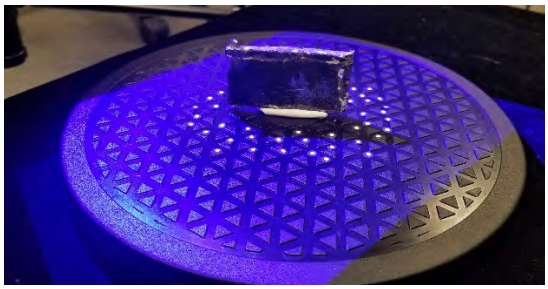

Figure 9. Steel shell being scanned in 3D to obtain coordinates of points on the steel shell surface.

The scanner generates (xyz) coordinates of points on the surface of the steel shell in the form of a large N x 3 matrix where N is the number of points scanned. This is commonly referred to as a point cloud. Figure 10 (a-d) shows steps that were carried out during post processing of the point cloud data using a photogrammetry software – CloudCompare developed by Daniel Girardeau-Montaut. The point cloud was imported to CloudCompare and cross sections were made through the cloud by extracting multiple slices from the sets of points. A polyline which wraps around the points as closely as possible was generated based on a concave-hull algorithm which is in-built into the program. This set of polylines was exported to MATLAB where thickness measurements along each polyline was made. Finally, an unevenness parameter which shows the degree of non-uniformity in shell thickness is computed statistically. In Figure 10, (a-c) show top area of the scanned shell surface while (d) shows top and bottom of a single polyline segment extracted from the overall shell as a subset of the shell.

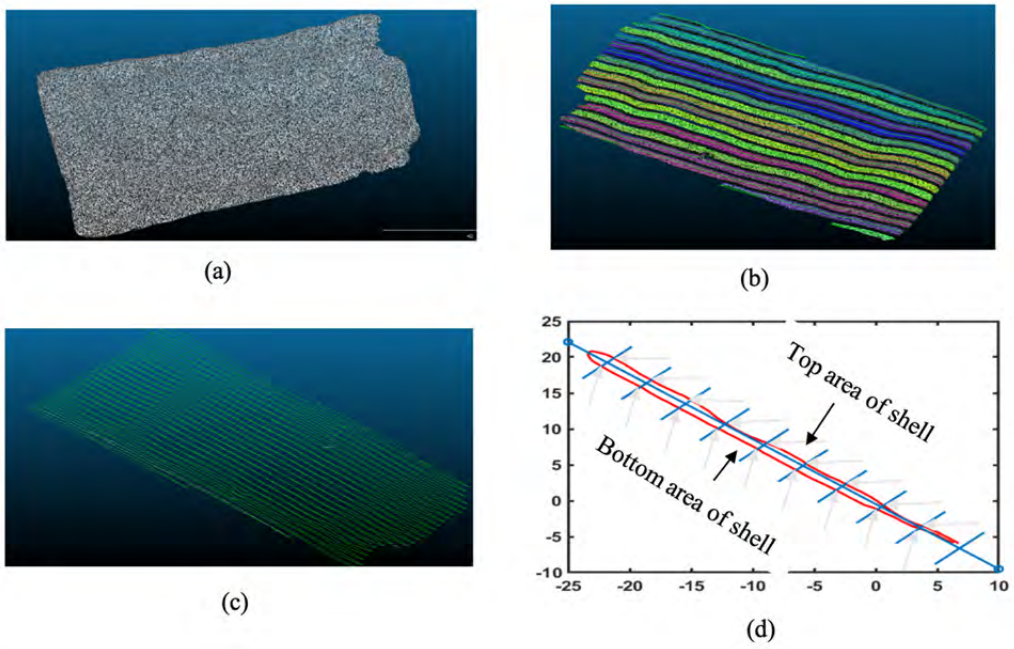

Figure 10 (a). Point cloud image as imported into CloudCompare from the 3D scanner. (b). Point cloud with sections made by making slices through the data points and creating a polyline wrapped around the points. (c). Polylines exported as a subset of the original cloud. (d). One Polyline data as exported to MATLAB for measurements.

Each slice of the polyline data is exported separately to MATLAB where thickness variations where calculated along the lengths of each polyline. It is clear from Figure 10(d) that the thickness can easily be computed as the distance between points on a Cartesian coordinate system. Figure 11 shows how the unevenness parameter in (2) was obtained for the shell.

Figure 11. One polyline with calculated d1, d2, and d3 values which represent thickness of three segments.

$$\frac{\sum_{i}^{n}\left(\frac{|d_i - d_{i+1}|}{li}\right)}{n} \qquad (2)$$

While much more work still needs to be done to prove out the overall experimental approach, the preliminary results suggest that mapping the thermal non-uniformitity associated with peritectic behavior using high resolution optical fiber temperature measurement is feasible. Our future work will focus on the use of a more closely spaced optical fibers to generate a full 2-D termal map of the shell growth during dip testing.

CONCLUSION

In order to demonstrate that a Rayleigh scattering based fiber-optic sensor can be employed to measure rapid thermal events near the surface of a copper mold, experiments were conducted to create localized temperature variations on copper test plate. Localized temperature variations were successfully measured with the fiber-optic distributed temperature sensor. Temperature features were used to approximate dimensions of hot and cold spots that were created by machining a pocket into the mold face. High spatial resolution and fast measurement rates by the fiber-optic system were obtained to produce thermal maps of the copper test plate. Moreover, experiments revealed that optical fibers require continuous thermal contact with the copper test plate for reliable temperature measurements. In addition to experimental simulations, a chill block dip test was conducted to test the measurement capability and survivability of optical fibers in the harsh environment of an induction melting furnace. Temperature profiles along the copper mold were successfully monitored during mold immersion in steel melt and solidification. Simultaneously, a shell characterization method was developed to directly observe the uneven shell deformation occurring from anomalous heat transfer between the mold wall and solidifying shell. In this method, 3D scanning data was post processed with CloudCompare and MATLAB to obtain a shell thickness unevenness parameter. From these measurements, an attempt will be made to match the unevenness parameter with mold thermal maps to determine the combined effects of alloying elements on the peritectic boundary shift in future work.

REFERENCES

1. M. Suzuki, C. H. Yu, H. Sato, Y. Tsui, H. Shibata, and T. Emi, “Origin of heat transfer anomaly and solidifying shell deformation of peritectic steels in continuous casting,” ISIJ Int., vol. 36, no. supplement, pp. 171–174, 1996.
2. Shepherd, R. & Knopp, I. & Brass, H.-G. (2012). Improved determination of the effect of alloying elements on the peritectic range in low-alloyed cast steel. Iron and Steel Technology. 9. 77-85.
3. K. E. Blazek, O. Lanzi, P. L. Gano, and D. L. Kellogg, “Calculation of the peritectic range for steel alloys,” Iron and Steel Technology, vol. 5, no. 7. pp. 80–85, 2008.
4. C. Steels, “Analysis of Heat Transfer and Solidifying Shell Deformation in Mold in High Speed Continuous Casting of Peritectic Medium Carbon Steels,” Steelmaking Proc., pp. 165–171, 1998.
5. G. Xia et al., “Investigation of mould thermal behaviour by means of mould instrumentation,” Ironmak. Steelmak., vol. 31, no. 5, pp. 364–370, 2004.
6. B. G. Thomas, M. A. Wells, and D. Li, “Monitoring Of Meniscus Thermal Phenomena with Thermocouples in Continuous Casting Of Steel,” in Sensors, Sampling, and Simulation for Process Control, John Wiley and Sons, 2011, pp. 119–126.
7. T. T. Natarajan, S. R. Story, T. J. Piccone, and K. D. Van Ness, “Peritectic Range Study Using Mold Thermocouple Data,” AISTech 2017 Proc., no. 412, pp. 1645–1654, 2017.
8. B. Lee, “Review of the present status of optical fiber sensors,” Opt. Fiber Technol., vol. 9, no. 2, pp. 57–79, 2003.
9. Y. Du, S. Jothibasu, Y. Zhuang, C. Zhu, and J. Huang, “Rayleigh backscattering based macrobending single mode fiber for distributed refractive index sensing,” Sensors Actuators, B Chem., vol. 248, pp. 346–350, 2017.
10. C. Zhu, Y. Zhuang, B. Zhang, R. Muhammad, P. P. Wang, and J. Huang, “A Miniaturized Optical Fiber Tip High-Temperature Sensor Based on Concave-Shaped Fabry-Perot Cavity,” IEEE Photonics Technol. Lett., vol. 31, no. 1, pp. 35–38, 2019.
11. V. Lecoeuche, M. W. Hathaway, D. J. Webb, C. N. Pannell and D. A. Jackson, "20-km distributed temperature sensor based on spontaneous Brillouin scattering," in IEEE Photonics Technology Letters, vol. 12, no. 10, pp. 1367-1369, Oct. 2000
12. X. Bao, J. Dhliwayo, N. Heron, D. J. Webb and D. A. Jackson, "Experimental and theoretical studies on a distributed temperature sensor based on Brillouin scattering," in Journal of Lightwave Technology, vol. 13, no. 7, pp. 1340-1348, July 1995.
13. K. Shimizu, T. Horiguchi, and Y. Koyamada, "Measurement of distributed strain and temperature in a branched optical fiber network by use of Brillouin optical time-domain reflectometry," Opt. Lett. 20, 507-509 (1995)

14. Y. Weng, E. Ip, Z. Pan, and T. Wang, "Single-end simultaneous temperature and strain sensing techniques based on Brillouin optical time domain reflectometry in few-mode fibers," Opt. Express 23, 9024-9039 (2015).

15. B. Guan, H. Tam, X. Tao, and X. Dong, “Simultaneous Strain and Temperature Measurement Using a Superstructure Fiber Bragg Grating,” in IEEE Photonics Technology Letters, vol. 12, no. 6, pp. 675-677, June 2000.

16. H. J. Patrick, G. M. Williams, A. D. Kersey, J. R. Pedrazzani, and A. M. Vengsarkar, “Hybrid fiber Bragg grating/long period fiber grating sensor for strain/temperature discrimination,” IEEE Photonics Technol. Lett., vol. 8, no. 9, pp. 1223–1225, 1996.

17. J. Jung, H. Nam, and B. Lee, “Fiber Bragg grating temperature sensor with controllable high sensitivity,” Conf. Proc. - Lasers Electro-Optics Soc. Annu. Meet., vol. 1, pp. 405–406, 1998.

18. B. Zhang and M. Kahrizi, "High-Temperature Resistance Fiber Bragg Grating Temperature Sensor Fabrication," in IEEE Sensors Journal, vol. 7, no. 4, pp. 586-591, April 2007

19. B. G. Thomas, M. K. Okelman,. Implementation Of Temperature and Strain Micro-Sensors into a Casting Mold Surface. in Sensors, Sampling, and Simulation for Process Control (pp. 127–134). John Wiley and Sons. 2011.

20. D. Lieftucht, M. Reifferscheid, T. Schramm, A. Krasilnikov, and D. Kirsch, “HD Mold – A New Fiber-Optical-Based Mold Monitoring System," Iron and Steel Technology. 10. 87-95, 2013.

21. T. Spierings, A. Kamperman, H. Hengeveld, J. Kromhout, and E. Dekker, “Development and Application of Fiber Bragg Gratings for Slab Casting,” AISTech 2017 Proc., pp. 1655–1664, 2017.

22. Y. Du et al., “Cryogenic temperature measurement using Rayleigh backscattering spectra shift by OFDR,” IEEE Photonics Technol. Lett., vol. 26, no. 11, pp. 1150–1153, 2014.

23. Y. seok Kwon, K. Naeem, M. Y. Jeon, and I. B. Kwon, “Enhanced sensitivity of distributed-temperature sensor with Al-coated fiber based on OFDR,” Opt. Fiber Technol., vol. 48, pp. 229–234, 2019.

